The International Journal of Advanced Manufacturing Technology (2023) 125:157–168
https://doi.org/10.1007/s00170-022-10697-z

ORIGINAL ARTICLE

Effect of preheating during laser metal deposition on the properties of laminated bending dies

Hamed Dardaei Joghan[1] · **Marlon Hahn**[1] · **A. Erman Tekkaya**[1]

Received: 12 July 2022 / Accepted: 9 December 2022 / Published online: 22 December 2022

Abstract
Metal-laminated tooling provides a fast and cheap manufacturing concept. In this study, laser metal deposition (LMD) is used for reducing and eliminating the stair step effect in a metal-laminated bending die. Preheating could decrease the undesired residual stresses in additive manufacturing, thus a systematical analysis of the effect of preheating of the laminae on the surface quality and mechanical properties of the bending die is performed. Ferritic steel sheets (S355 MC) with a thickness of 2 mm are laser cut and stacked up to manufacture the laminated bending die with a radius of 6 mm. The sheets are joined and the stair steps are filled with LMD with stainless steel powder 316L-Si. The initial temperature of the tool sheets (substrates), beside room temperature, is elevated up to 300 °C. The effect of the preheating on the surface roughness, shape deviation, hardness, and residual stresses of the die are investigated. The mean height of the surface increases by 59% at elevated temperatures. However, the tensile residual stress parallel to the weld direction at the middle of the deposited area decreases only around 25%. The functionality of the forming tools manufactured by this method is proven by bending of DC06 and HC380LA sheets.

Keywords Additive manufacturing · Laser metal deposition · Laminated tooling · Rapid prototyping · Sheet metal forming · Surface roughness

1 Introduction

Laminated metal tooling as a rapid tooling concept reduces manufacturing costs and lead time. In laminated manufacturing, sheets are cut by laser or waterjet and stacked to create the final geometry of the target tool in a discretized manner. Layered manufacturing offers the possibility of flexible material selection, installation of sensors and smart tooling [1]. The initial idea of laminated tooling was patented by Hart F.V. [2] for manufacturing shoe molds. Clevenger et al. [3] patented this method for manufacturing laminated hydroforming tools. From the beginning of the 1980s, metal-laminated tooling is used in the automotive industry [4] where this method is used for manufacturing of blanking tools. The application of laminated tooling for building angular or curved surfaces leads to inhomogeneous and serrated surfaces known as the stair step effect. This disadvantage is a function of the layer thickness and angle of surface where a higher layer thickness means a rougher surface roughness. Different methods are proposed for eliminating this effect. Kunieda and Nakagawa [5] used the machining method for eliminating the stair step effect for manufacturing metal laminated deep-drawing tools. The application of the beveled edge was patented by Weaver [6] for laminated hydroforming tools. Yoo and Walczyk [7] established an automatic advanced slicing model for a beveled edge laminated forming tool. Walczyk and Hardt, 1998 [8] showed a successful but complex and costly method of combining beveling and machining of the edges of laminae for manufacturing stamping dies. An intermediate layer (elastomer or soft sheet metal) among the laminated deep-drawing tool and the blank to lower the stair step effect was used by Kleiner and Krux [9]. The study showed that this method can provide the required form and dimension accuracy. Galvanizing of contours is another possibility of generating a homogenous surface [10] but it needs several thermal cycles. Yoon and Na [11] eliminated the stair step effect by laser brazing and soldering. It is concluded that the surface has a

✉ Hamed Dardaei Joghan
Hamed.Dardaei@iul.tu-dortmund.de

[1] Institute of Forming Technology and Lightweight Components, TU Dortmund University, Baroper Str. 303, Dortmund, Germany

low hardness and the addition of hard particles is not negligible but the need for machining for improving the surface roughness is unnecessary. Hiegemann et al. [12] used a roller burnishing tool for smoothing the stair steps of low carbon steel. Even though the hardness of the smoothed surfaces due to the strain hardening increased, it is not enough for the tooling requirements. Another solution for reducing the stair step effect is the application of additive manufacturing (AM) processes, such as laser metal deposition (LMD). Laser cladding or LMD is a subdivision of Direct Energy Deposition (DED) of the AM method based on the standard DIN EN ISO/ASTM 52,900 [13]. The principle of the laser metal deposition is illustrated in Fig. 1. In LMD, the metal powders are introduced into the focal point of the laser beam with the aid of inert gas (e.g. argon). In the shielded atmosphere (argon gas), the temperature of metal powder reaches the melting point and the molten material is deposited on the surface. In 1997, for the first time, Erasenthiran et al. [14] investigated on a small extent the usage of laser cladding for reducing the stair step effect. In this study, two methods of Ni-powder feeding is used, replaced-powder and blown-powder. The study noted that the blown powder parts show a lower porosity and better surface quality. The application of combined AM and roller burnishing as a hybrid additive manufacturing method was patented by Hölker-Jäger et al. [15]. Dardaei Joghan et al. [16] showed a successful utilization of LMD for manufacturing of metal laminated deep drawing tools. Therein, three different post processing methods, namely milling, ball burnishing, and laser polishing, were investigated to improve the surface roughness. It is shown that the new process route enables the production of rapid tooling of complex geometries with enhanced cooling or heating channels and functional elements. Souza et al. [17] studied the improvement of the surface roughness by laser polishing with maximum laser power of 500 W. It is observed that the surface roughness can be effectively

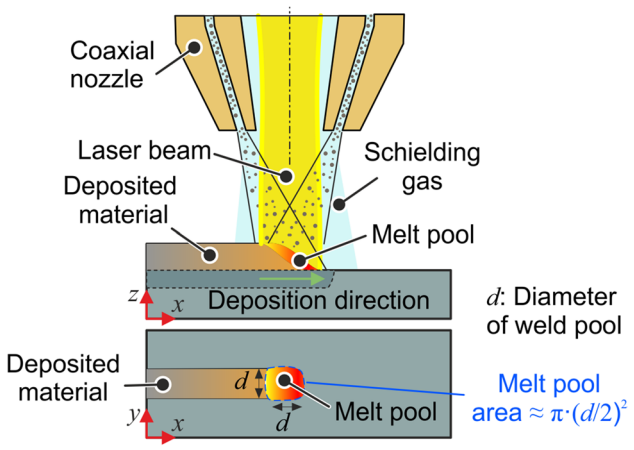

Fig. 1 Principle of laser metal deposition

improved by 86% with an insignificant decrease in the hardness of the deposited surface. Barragan De Los Rios [18] showed that the surface roughness of a bimetallic part deposited from AISI 1045 and 316L SS can be improved by high speed milling by a minimum of 90% in both deposited areas.

Residual stresses, surface roughness and shape accuracy are the main challenges by using AM for laminated tooling. Residual stresses in additively manufactured parts are not only dependent on the process parameters such as power, feed rate, and mass flow, they also highly depend on scanning strategies, cooling times or dwell time, and the initial temperature of the substrate [19]. Rangaswamy et al. [20] showed that the laser rastering direction has an insignificant effect on the magnitude of the residual stresses of 316L powder. Wang et al. [21] showed that the cooling times' effect on residual stress depends on the deposited material. It is shown that a longer cooling time for deposited Inconel 625 material leads to lower residual stresses. However, for deposited Ti64 material, this happens by a shorter cooling time.

Preheating of the substrate in AM is one solution for reducing undesired residual stresses of the produced parts [22]. The preheating of a bulk substrate out of die steel Cr12 (1.2080) reduces the maximum residual stress of Co-based alloy powder from 350 MPa at room temperature (RT) to only around 280 MPa at 600 °C (around 20% reduction) in the deposited surface. However, this value for the die steel powder (Cr12MoV) is only 6% and for nickel-based powder Ni60A, it has no significant influence [23]. Alimardani et al. [24] showed that preheating of the bulk substrate heat-treated steel (36CrNiMo4) leads to a uniform and dendritic structure of deposited layers compared to a non-preheated substrate for Co-alloy powder (Stellite®1). Ding et al. [25] determined the increase of the ferrite content of low-alloy steel powder (12CrNi2) by preheating the substrate and consequently decreasing the hardness of the deposited surface. The preheating also avoids crack initiations in joining dissimilar materials in LMD as shown by Meng et al. [26] for 316L and Inconel625. The study also proved that the preheating by so-called laser synchronous can improve the microstructure. The laser synchronous heating method is heating of the substrate or deposition area with a laser before the application of the initial or next deposition layer.

The literature review shows the potential of using LMD for reducing the stair step effect of laminated tools. One of the advantages of eliminating the stair step effect by LMD is the high hardness, which omits the necessity of an additional hardening process. Since in conventional hardening processes the whole tool needs to be heated, the application of locally concentrated energy in LMD is energy-saving and emits less CO_2 which is important for green manufacturing. The preheating of the laminae during LMD influences the mechanical properties. The literature review indicated that there is no existing study in the field that investigates the

effects of preheating on the surface roughness of segregated surface sheets deposited by laser deposition. Therefore, in the following sections, its effect on surface roughness, hardness, and residual stresses of the deposited surfaces of a bending die will be discussed. At the end, the resulting form accuracy and surface roughness of bent sheets of two different materials, high strength steel HC380LA and DC06, are discussed.

2 Experimental work

High-strength ferritic sheets, S355MC, with a thickness of 2.0 mm with a yield strength and tensile strength of 396 and 487 MPa respectively (chemical composition provided in Table 1) are laser cut and stacked to build a laminated bending die with a die radius of 6 mm. The LMD is succeeded by the Lasertec 65 3D hybrid machine by Sauer GmbH/DMG MORI AG. It has a 2.5 kW fiber-coupled diode laser and a coaxial powder nozzle (COAX9 — 1.6 mm) with Argon gas for shielding. For LMD, the laser is used as energy source and powder as the deposited material. The sheets are welded with powder 316L-Si (1.4404) with a particle diameter of about 45–125 µm. The composition of the powders and the melting temperature are provided in Table 2. The weld geometries are measured by a ZEISS AXIO IMAGER M1m reflected light microscope with 50× magnification. The µsoft analysis software is used for the calculation of the surface roughness parameters in the radius direction. The profile parameters are calculated based on the standards DIN ISO 4287 [27] and DIN ISO 25178–2 [28]. In the 2D direction the roughness parameters R_a and R_z, which represent the arithmetical mean deviation and the maximum height of the profile respectively, are determined. The main disadvantage of the two-dimensional profile parameters especially by tactile measurement is a dependency of the results on the measured position. To avoid this problem, the optical measurement offers the possibility of the determination of the 2D surface parameters along more than one line. In this paper, for the 2D surface parameters, 50 lines are defined for the calculation of the mean value. Since the surface topography is inherently three-dimensional, the 2D surface parameters provide only insufficient information regarding the real surface roughness [29]. Therefore, in the 3D space, besides the arithmetic mean of the absolute height (S_a), the core roughness depth (S_k) are also calculated. The summation of the maximum peak and the minimum valley in the determined area (S_z), an extension of the R_z, is calculated. The main surface irregularities based on [30] are divided into three categories: (I) roughness, (II) waviness and (III) error of the form. Hence, W_a, which is the arithmetic mean deviation of the wave height, is also calculated. All parameters are calculated with a Gaussian filter with a wavelength of 0.8 mm in the radius direction. Vickers hardness measurement is realized by a Wolpert Diatestor 2 RC/S hardness machine with an indentation force of HV0.1 (load test: 980.7 mN). Since a hardness measurement on the curved surface leads to inhomogeneous penetration (inaccurate results), the bending tools for the hardness measurement are cut (perpendicular to the weld), grinded, and finally polished with 1 µm diamond suspension. The residual stresses are measured by the G2R model machine from Stresstech GmbH with an X-ray source of Cr-tube with a collimator diameter of 2 mm. Based on [31] the 2θ angle 152.3° with an X-ray voltage of 30 kV and a current of 8 mA are selected. The measurement was performed parallel and perpendicular to the weld track. The modified-chi measuring method with a tilt angle of 42° with ± 3° tilt oscillation in 8 angles (± 19.5°, ± 28.2°, ± 35.4 °, ± 42°) with an exposure time of 20 s is used.

The depositing of material is divided into two steps: (I) bonding, and (II) filling (Fig. 2a). This is to avoid undesired thermally induced deformation of the sheets. The sheets are preheated with the help of two heating cartridges as shown in Fig. 2b. A 1 mm cover sheet is used for providing a homogenous heat transfer for all sheets (Fig. 2c). Besides the room temperature, the initial temperature of the tool sheets is elevated at 100 °C, 200 °C and 300 °C. The process parameters for LMD in the bonding step and filling step are presented in Table 3. In the filling step, a weld overlapping of 0.56 mm is utilized.

Each experiment is repeated three times, giving a total of 12 runs. A unidirectional strategy is used for the filling step. During the preheating, the temperature of the sheets is monitored by a thermometer. Due to safety and technical

Table 1 Chemical composition in % and melting temperature in °C of the tool sheet

	C	Mn	Si	P	S	Nb	v	Ti	Melting temperature
S355MC (1.0976)	0.12	1.5	0.5	0.025	0.02	0.09	0.2	0.15	1480–1526 °C

Table 2 Chemical composition in % and melting temperature in °C of the 316L-Si powder

	C	Ni	Cr	Mo	Si	Mn	Fe	Melting temperature
316L-Si (1.4404)	0.03	12.0	17.0	2.50	2.30	1.00	rest	1400 °C

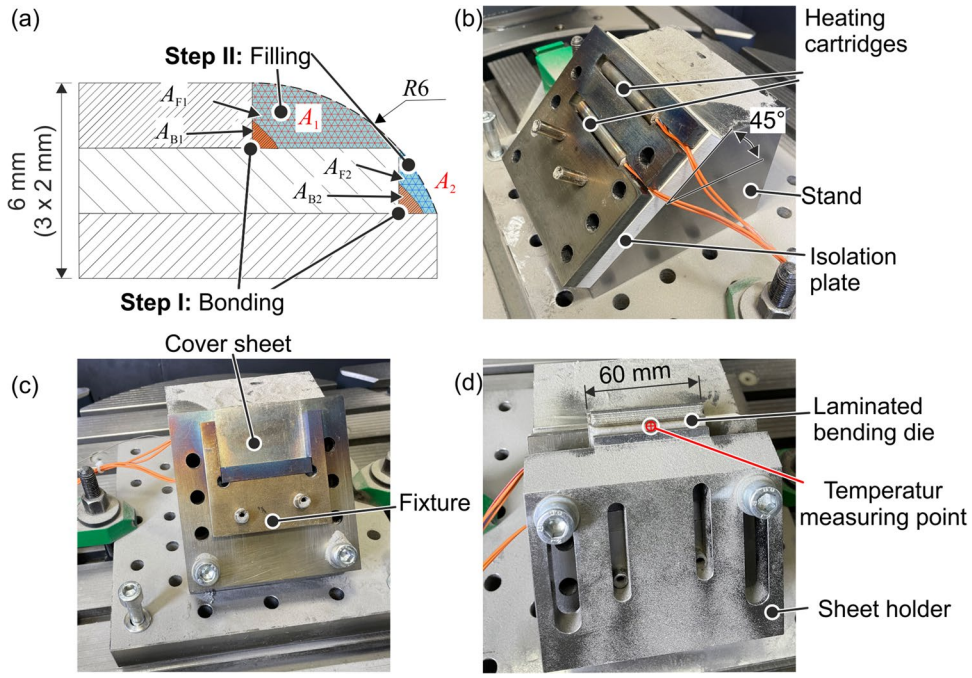

Fig. 2 (**a**) Sheet combination and deposition strategies, (**b**) preheating setup, (**c**) laminated bending die positioning, (**d**) laminated bending die after LMD

Table 3 Process parameters for LMD

	Power (P) in W	Feed rate f in mm/min	Powder mass flow $\dot{m}$ in g/min
Bonding step	1400	1000	7
Filling step	1000	1400	4

issues, the preheating is ended just before the LMD process. During LMD, the temperature and size of the melt pool are recorded. During the deposition, the stair steps are divided in two areas $A1$ and $A2$. Each area has its corresponding bonding area (B) and filling area (F). Thus, the whole stair step is divided in 4 sections named as A_{B1}, A_{F1}, A_{B2} and A_{F2} as shown in Fig. 2a. An embedded camera on the laser head allows the measurement of the melt pool size and temperature using image processing. The E-AqS (melt pool temperature measurement system) is developed by the Frauenhofer Institut IWS Dresden. The acquired data is directly post-processed with DMG MORI's AMAnalyser software.

Electron backscatter diffraction (EBSD) measurements are performed with a Mira-3 device from the company Tescan GmbH. For the measurements, the voltage of 15 kV and a magnification of 1000 is used. Air bending experiments (unsymmetric, with one side fixed) are performed in a Zwick250 universal testing machine. The test setup is shown in Fig. 3a. HC380LA and DC06 blanks with a thickness of 1 mm are used for the bending experiments. For characterization purposes, tensile experiments for both blanks based on the standard DIN EN ISO 6892–1 [32] are performed. The tensile specimens are laser cut according to the standard DIN 50,125 [33]. For the bending experiments, the sheets are laser cut in the rolling direction with a width of 40 mm. The sheets are bent with a bending angle of 90° with a punch velocity of $v = 5$ mm/s (see Fig. 3b). The blanks are clamped between the laminated bending die and the blank holder, where the blank holder force realized by screws. The clearance between the non-laminated punch and the laminated bending die was 1 mm.

3 Results and discussion

3.1 Effect of preheating on surface roughness

The final surface roughness of the formed parts is directly influenced by the surface roughness of the forming tool which are directly in contact with the specimen. In order to investigate the influence of preheating on the quality of the manufactured tool surfaces, various roughness parameters of laminated tools are measured. Normally, rather low values of R_i/S_i etc. (Fig. 4a) are desired for a forming tool, which can be adjusted in the conventional case by machining. Therefore, for the proposed tool concept, the surface roughness values resulting from the LMD process are considered. Figure 4b shows the results of the surface roughness parameters in the 2D direction, where the preheating temperature has no significant effect on the R_a values. However, a decrease in the maximum height of the profile (R_z) by around 30% at 300 °C is observed. Considering the 3D areal surface parameters shows that S_a increases by 31% (Fig. 4c). The decrease

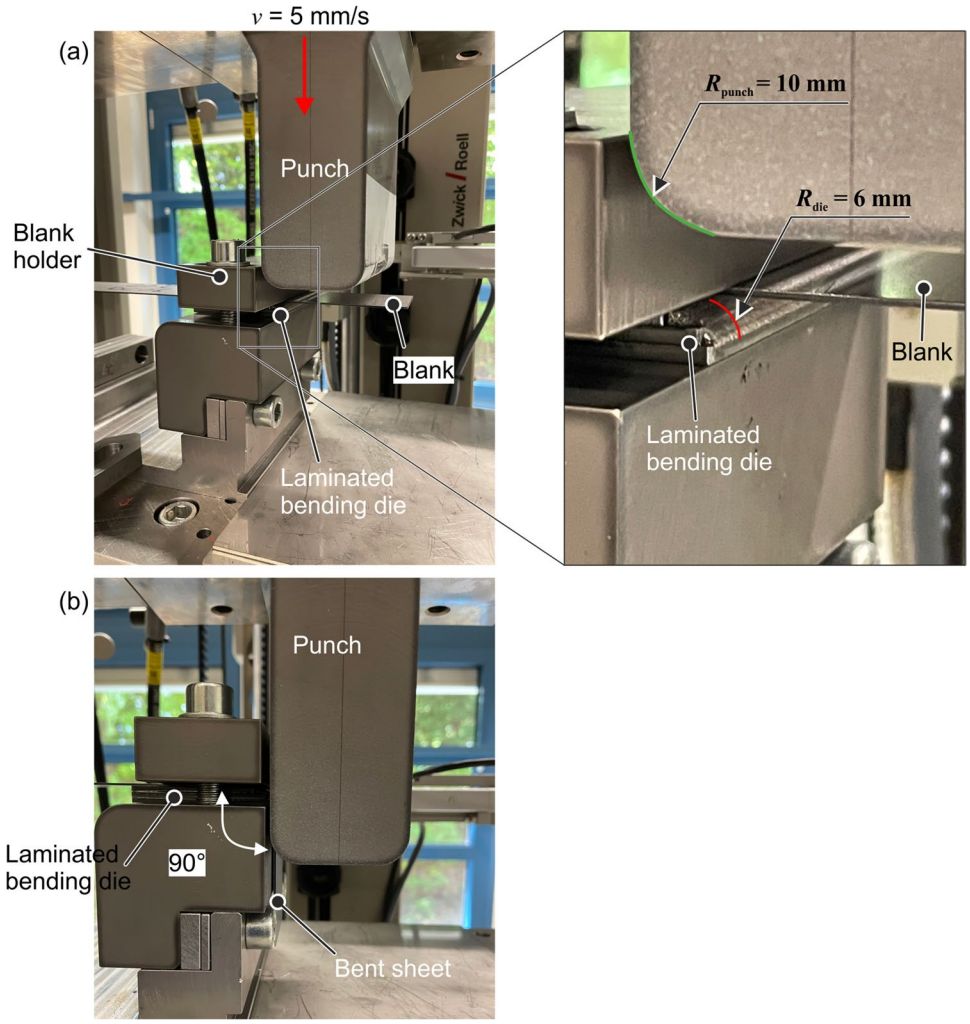

Fig. 3 (**a**) Air bending test setup, (**b**) after bending

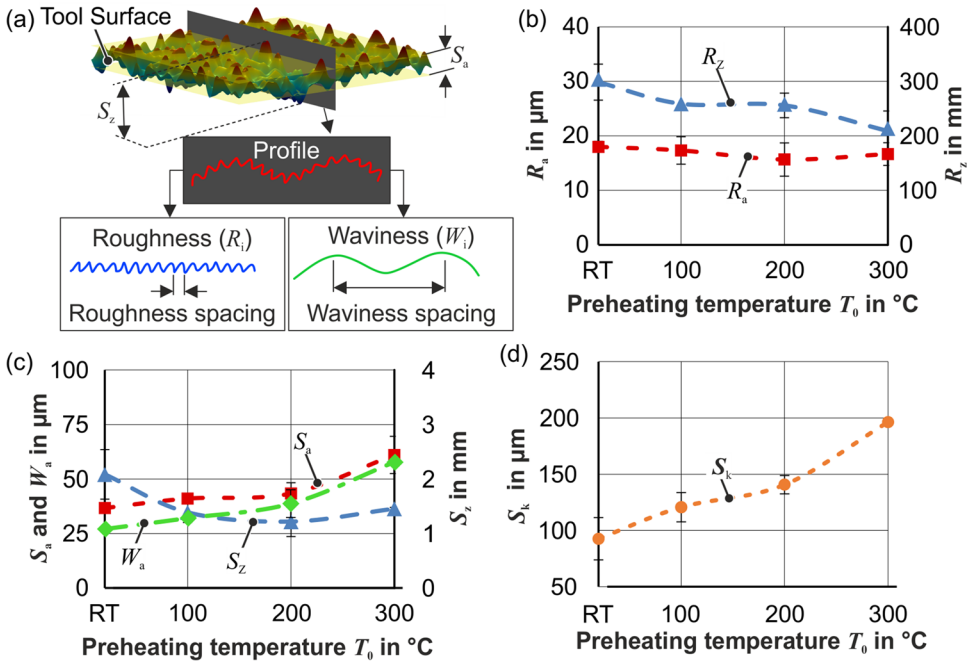

Fig. 4 (**a**) Definition of profile, roughness and waviness, pre-heating temperature effect on (**b**) R_a and R_z,(**c**) S_a,S_z, waviness parameter W_a, (**d**) core height S_k

in S_z is the same as R_z in 2D. So, the preheating temperature leads to fewer peaks on the surface due to a low cooling rate and a further semi-solid state in the melt pool. The long time semi-solid state also causes the waviness of the surface (Fig. 4c). The waviness of the surface increases up to 100% by elevating the preheating temperature. Figure 5 illustrates the mean profile height (h_m) of the surface of the deposited areas along the radius at different preheating temperatures. The profile length is cut for all profiles at the same place for the length of 6 mm. By elevating the preheating temperature, the height of the wave domains is increasing. At elevated preheating temperatures, the mean profiles are smoother with a longer length and higher wave domain compared to the profiles at RT. At RT, there are more small and sharp picks because of the fast cooling rate.

In Fig. 4d, the S_k course for different preheating temperatures is presented**.** S_k represents the core surface roughness of the bearing area (the area of contact between tool and blank) after the primary operating cycle such as bending experiments. The preheating temperature rises the S_k depth which leads to higher friction forces during forming operations between tool surface and blank surface after the primary operating cycle and consequently leads to higher process forces during the forming operation.

3.2 Effect of preheating on residual stress

The residual stresses induced by manufacturing processes play an important role in the operating life of tools or parts. Almost all manufacturing processes cause different states of residual stresses in the parts. In metal forming tools, compressive residual stress is mainly desired since it increases the fatigue life of the tool by stopping crack growth [34]. Rapid heating, cooling, and remelting with simultaneous melting of the previous solidified deposited materials lead to particular thermal cycles in AM-metal parts. Such a severe thermal cycle could lead to sharp compressive or tensile residual stress gradients, which could result in local failures in the manufactured parts [22]. In the present work, the residual stress is measured in two directions, one parallel to the weld line ($\sigma_{0°}$) and perpendicular to the weld line ($\sigma_{90°}$) in both the weld and heat affected zone (HAZ). The measurement for each point is repeated for three samples for each temperature, and the standard deviation for three measurements is calculated. In the deposited area, the residual stresses under 90° are all positive (tensile stresses) as demonstrated in Fig. 6a. The residual stresses along the weld line ($\sigma_{0°}$) at RT and 300 °C are negligible but at 100 °C and 200 °C, the values are positive but still lower than the residual stresses at 90°. The preheating temperature can reduce the tensile residual stress by a maximum of 25% at 100 °C compared to RT perpendicular to the weld track ($\sigma_{90°}$). The tensile strength and ultimate strength of the 316L tensile samples manufactured by DED methods are 486 and 676 MPa respectively [35]. Considering the tensile strength of the deposited material, elevating the initial temperature of the tool sheets during LMD can reduce the negative effect of the tensile residual stresses on the tool surface, but only by max. 25% at 100 °C.

The positive residual stresses perpendicular to the weld line ($\sigma_{90°}^{Weld}$) could be explained by the rapid thermal cycles which consist of two phases of heating and cooling as

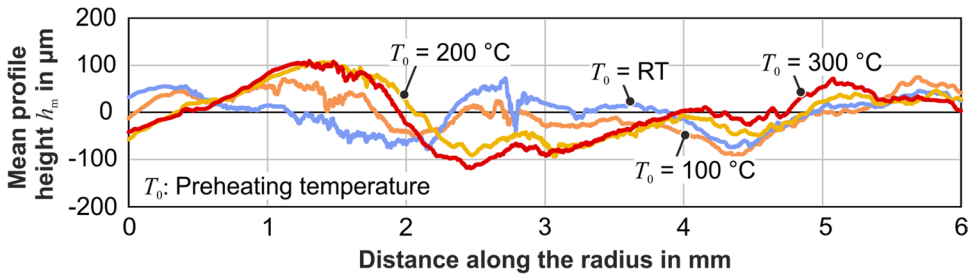

Fig. 5 Preheating temperature effect on mean profile height h_m

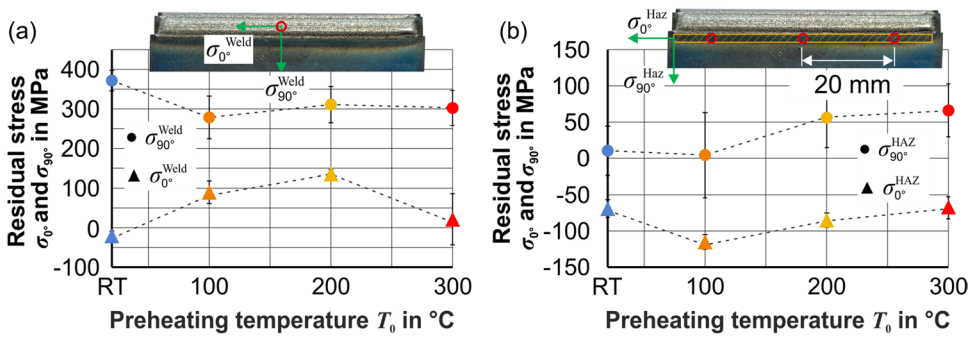

Fig. 6 Preheating temperature effect on residual stress in (**a**) weld area, (**b**) HAZ

mentioned. In the heating phase, the laser (energy source) heats both the powder material and substrate, which leads to an expansion in the molten material. But this expansion is limited by the deposited or substrate material around the heated zone, resulting in the formation of compressive stresses. Directly after removal of the laser, the cooling phase begins, where the material and the heated zone cool down and the deposited material starts to shrink. This shrinkage is gradually reduced by plastic deformation developed during the heating phase. During the resolidification of the deposited material, it tends to shrink but is partially retained by the previously deposited material, resulting in tensile residual stresses [22].

In the HAZ (Fig. 6b), the residual stress at RT is almost zero in both directions. By increasing the temperature from 100 °C on, the residual stresses increase at 90° ($\sigma_{90°}^{Haz}$) and reduce at 0° ($\sigma_{0°}^{Haz}$). Since the HAZ is subjected to much lower thermal cycling and has a free length (beginning and finishing points of the weld tracks) on both sides for thermal expansion, the residual stresses are comparatively low and negligible. The same is valid for residual stresses in the deposited area parallel to the weld tracks ($\sigma_{0°}^{Weld}$).

3.3 Effect of preheating on shape accuracy and hardness

The accuracy of the formed blanks' geometry is directly affected by the tool shape accuracy. Conventional manufacturing processes such as milling, due to the accurate moving of the cutting tool and material-removing process, deliver a high geometry accuracy which is not the case in most common AM processes. In laser metal deposition, the geometry accuracy is dependent on the geometries of deposited tracks. Heat transfer and solidification are two important physical phenomena affecting the size and geometry of the deposited tracks. Figure 7 shows metallographic image results for the manufactured bending dies. It can be seen that in all investigated cases, there is an inaccuracy in the die radius. At RT, the deposited material is not completely covered over the whole radius. This problem decreases by increasing the preheating temperature, and for 300 °C, there is even excess-deposited material.

This phenomenon can be explained by studying the melt pool size shown in Fig. 8a and b. The influence of the preheating temperature on the melt pool size is significant and increases by rising the preheating temperature. The size of the melt pool (see Fig. 1) in the bonding step increases by elevating the preheating temperature for A_{B1} and A_{B2} around 48% and 62% respectively (Fig. 8a). The small difference in the size of the melt pool in the areas A_{B1} and A_{B2} is due to the temperature elevating in the tool sheets (substrate) during the welding of A_{B1}. The effect is more significant for the melt pool size in the filling step (Fig. 8b) where the melt pool size of A_{F2} is higher than A_{F1}. The size of the melt pool of A_{F2} is more than twice as high at the same preheating temperature compared to A_{F1}. The melt pool size deviation

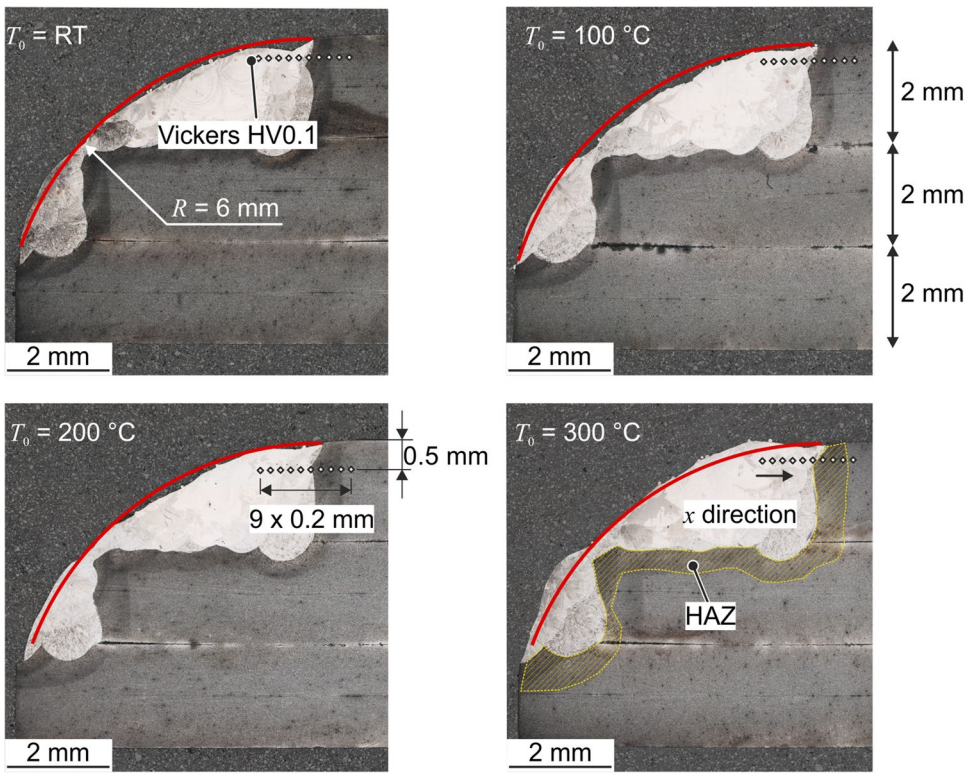

Fig. 7 Preheating temperature effect on shape accuracy of the die radius of 6 mm

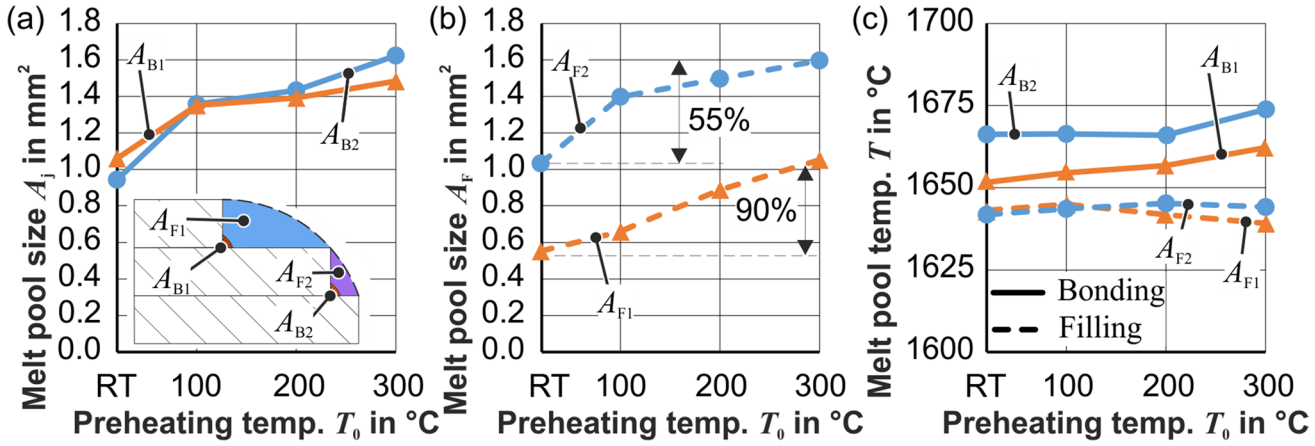

Fig. 8 Preheating temperature effect on (**a**) melt pool size for bonding step, (**b**) melt pool size for filling step, (**c**) melt pool temperature T

at RT varies around 34 to 40% in the filling step. However, this deviation is reduced to a maximum of 27% at elevated temperatures, which shows a more stabilized melt pool size at elevated temperatures. The melt pool size in A_{F1} increases by a maximum of 90% at 300 °C compared to RT (Fig. 8b), which for A_{F2} is 55%. The mean melt pool temperature (T) is ca. 1642 ± 2 °C for all temperatures (Fig. 8c). Overall, the elevated preheating temperature has no significant effect on the melt pool temperature but the melt pool size increases, which then leads to over dimensioning at 300 °C.

Forming tools manufactured by conventional methods need to be hardened due to high process forces during the forming process. Metal-AM parts, due to thermal cycles and alloying elements, can offer a high hardness. The value of the hardness depends on the AM process parameters and chemical composition of the weld and substrate material. Figure 9 shows evaluation of the hardness of the manufactured bending dies along the x-direction that goes from the deposited area to the tool sheets. The hardness profile is quantitatively in agreement with results for LMD for single weld tracks [36] and multi-weld tracks [37]. In the deposited area, by elevating the temperature, the hardness decreases due to the gradual cooling rate of the melt pool in the deposited area, which leads to the formation of bigger grain sizes (see Fig. 10a). The results of EBSD (see Fig. 10a) confirm that the grain size of the deposited area for all temperatures is coarser than in the HAZ and transition zone. It can be seen that for all temperatures, the grain size at HAZ and transition zone is on average around 33% of the grain size of the deposited area (see Fig. 10b). There is no significant hardness difference between 100 and 200 °C however, at 300 °C the hardness decreases ca. 19% compared to RT.

According to Ya et al. [36] and Hao et al. [37], the reason for such a high hardness course in the transition zone also could be a formation of the alloying elements in this area. The results of EDX of 316 SS powder shows that after the transition zone the percentage of alloying elements (nickel and chromium) decreases sharply which leads to a lower hardness as reported by [18].

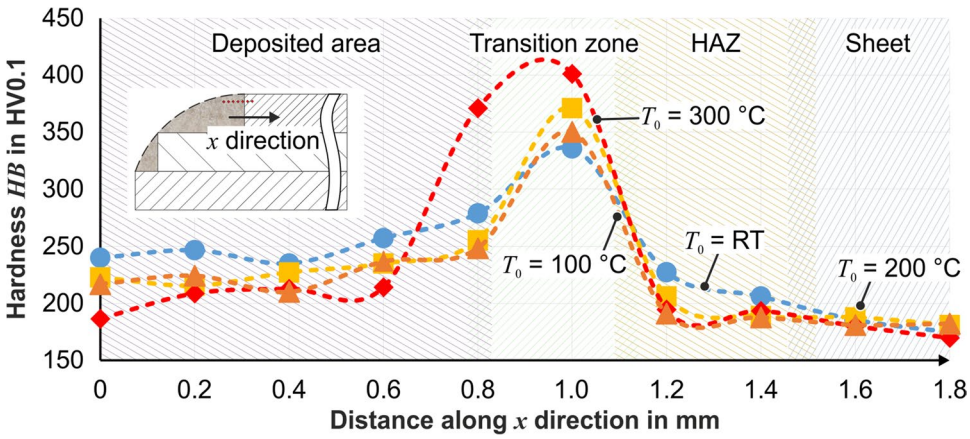

Fig. 9 Preheating temperature effect on hardness of deposited materials

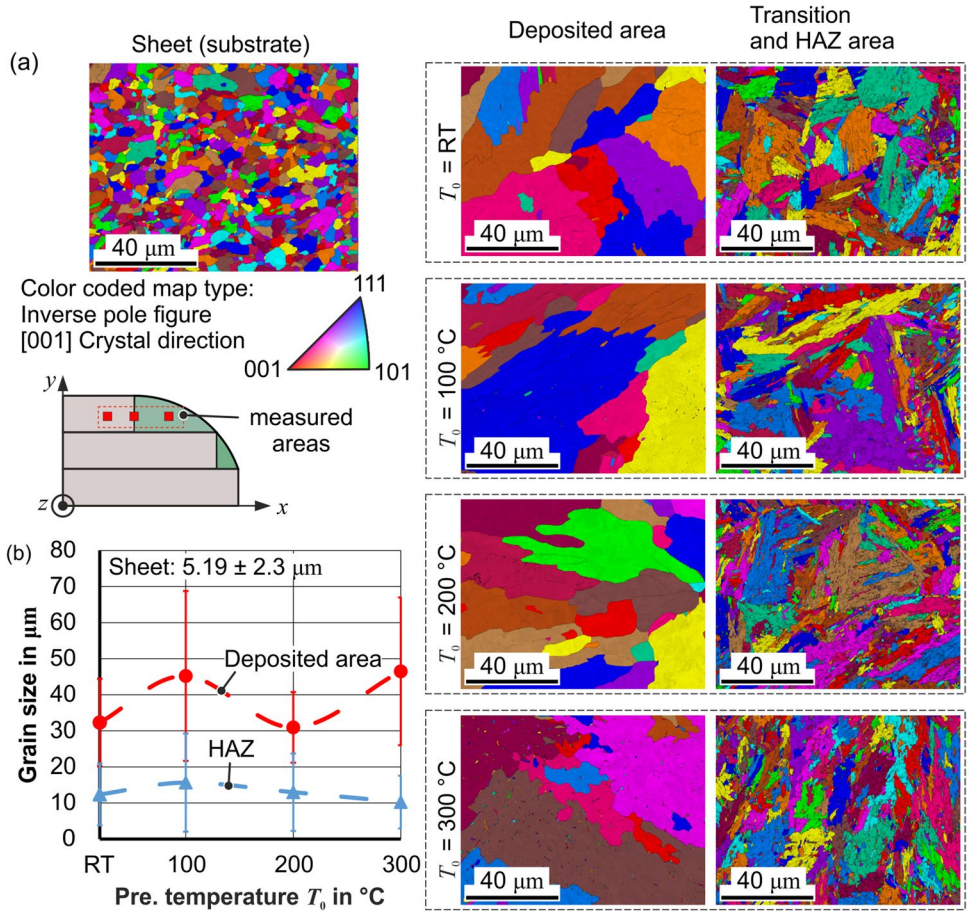

Fig. 10 EBSD results for different depositions and HAZ areas for different temperatures

3.4 Effect of preheating on bending radius

Bending experiments are conducted to analyze the effect of the various achieved tool surface roughnesses due to the preheating temperatures on the bending result of the two different blank materials. For calculating the radius right at the end of the bending process (before unloading), the springback effect is omitted, i.e. subtracted from the measured part radius after unloading. Since the width ($b = 40$ mm) to thickness ($t = 1$ mm) ratio of the blank is high, a plane strain state is considered. By using a Poisson's ratio of 0.3 and replacing the width and thickness values, the mean radius change (Δr_m) due to springback is calculated from the classical bending theory as:

$$\triangle\left(\frac{1}{r_m}\right) = \frac{1}{r_m} - \frac{1}{r'_m} = 0.273 \cdot \frac{M_b}{E} \text{ with } M_b = \frac{1}{2\sqrt{3}}\sigma_f b t^2 \quad (1)$$

where r'_m is the bending radius after unloading, M_b the bending moment, E the Young's modulus of the blank equal to 210 GPa, and σ_f is the flow stress of the blank material. Since the bending leads to strain hardening, the corresponding flow stress is determined with the calculation of the bending equivalent plastic strain ($\bar{\varepsilon}_{Plastic}$). The equivalent plastic strain at the inner radius of the bent sheet, by considering the plane strain state, is equal to $\bar{\varepsilon}_{Plastic} = \frac{2}{\sqrt{3}}\left|\ln\left(1 - \frac{0.5}{5.5}\right)\right| = 0.095$. The flow curves for the two used blanks from the tensile tests are presented in Fig. 11.

The flow stress (σ_f) of DC06 and HC380LA for $\bar{\varepsilon}_{Plastic} = 0.095$ is 310 and 491 MPa respectively. The calculated inner radius (r_i) before unloading for different

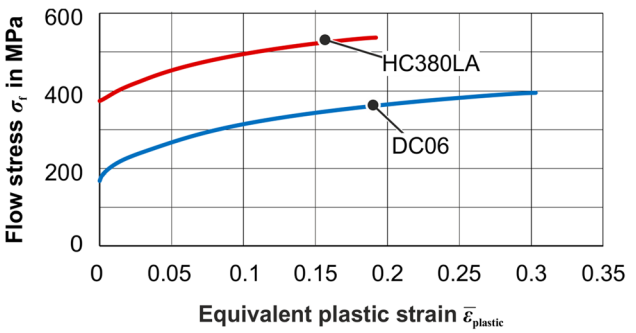

Fig. 11 Flow stress results for DC06 and HC380LA blanks in rolling direction at room temperature

preheating temperatures is presented in Fig. 12a. At RT, the calculated inner radius shows a maximum deviation from the (theoretically) desired value of 10% and 8% for HC380LA and DC06 accordingly. At 300 °C, the maximum inner radius deviation is only 2%. The reason for this deviation at RT is a smaller die radius because of missing deposited material (Fig. 7).

Figure 12b and c presents the surface roughness of the bent sheets for dies with different preheating temperatures. By considering the spread of the maximum mean surface roughness (R_a) and of the maximum height of the profile (R_z) of the bent sheets along the radius direction for both DC06 and HC380LA sheets, it could be concluded that the preheating temperature has not a significant effect on the surface roughness of bent sheets (Fig. 12b and c).

4 Conclusion

The surface quality and mechanical properties of laminated bending dies at different preheating temperatures of the laminae during the connecting laser metal deposition (LMD) are investigated. The stair step effect of laminated bending dies is successfully reduced by LMD with 316L powder. Besides the room temperature (RT), the laminae are preheated up to 100 °C, 200 °C, and 300 °C. The preheating leads to a reduction of the arithmetical mean deviation (R_a) and the maximum height of the profile (R_z) but simultaneously increases the waviness of the die surface. The residual stresses at the middle of the weld track in perpendicular direction at all temperatures are tensile (positive) and they are reduced only by 25% at 100 °C. The preheating also reduces the hardness of the deposited surface by 19%. At RT, more weld tracks are required for the complete filling of the die radius since the melting pool size is smaller than at elevated temperature. The bending experiments for two different sheet types, DC06 and HC380LA, show a maximum deviation of 8% (DC06) of the resultant inner radius of the bent sheet from the nominal radius. Consequently, without further knowledge about the wear of the tools in mass production for the different preheating temperatures, even the introduced tool without preheating suffices at least in efficient prototyping applications.

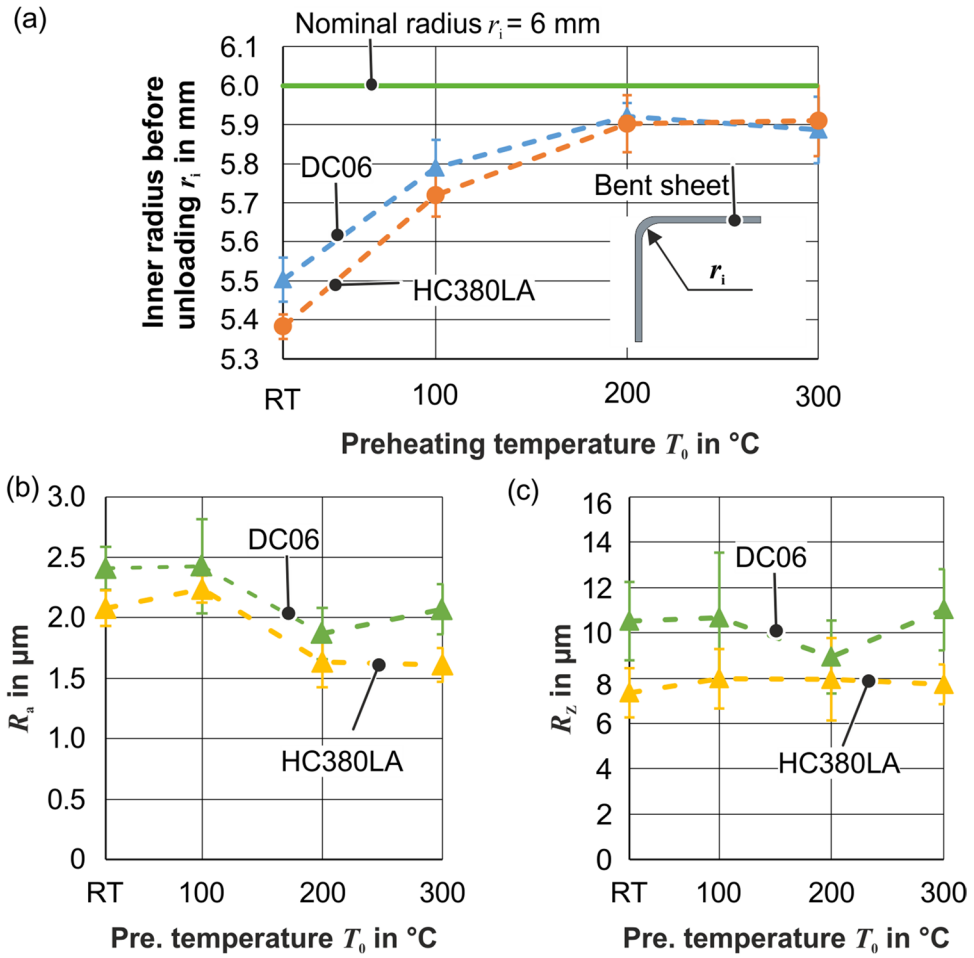

Fig. 12 Preheating temperature effect on (**a**) inner radius of bent sheets, (**b**) maximum mean surface roughness, R_a, (**c**) maximum height of the profile, R_z of bend sheets

Acknowledgements The authors would like to kindly acknowledge the support of the German Research Foundation (DFG). Mr. Sven Lukies is acknowledged for his technical support in metallography.

Author contribution Conceptualization: Dardaei Joghan H, Hahn M and Tekkaya AE; Methodology: Dardaei Joghan H and Tekkaya AE; Validation: Dardaei Joghan H; Experimental: Dardaei Joghan H; Writing (original draft preparation): Dardaei Joghan H; Writing (review and editing): Dardaei Joghan H, Hahn M and Tekkaya AE; Visualization: Dardaei Joghan H; Supervision: Hahn M and Tekkaya AE; Project administration: Dardaei Joghan H, Hahn M and Tekkaya AE; Funding acquisition: Dardaei Joghan H and Tekkaya AE.

Funding Open Access funding enabled and organized by Projekt DEAL. This study is a part of the project "Reducing the stair step effect for dies manufactured by layer-laminated manufacturing by additive and formative post-processing" with funding number 426515407. It is supported by the German Research Foundation (DFG).

Data availability Data and material are not provided with this article.

Declarations

Competing interests The authors declare no competing interests.

References

1. Cao J, Brinksmeier E, Fu M et al (2019) Manufacturing of advanced smart tooling for metal forming. CIRP Ann 68:605–628. https://doi.org/10.1016/j.cirp.2019.05.001
2. Hart FV (1942) Mold and mold making method: U.S. patent: 2274060 A, priority date: 31.10.1938(2274060)
3. Clevenger WS, Cohen JS, Cohen SG (1954) Laminated die form and method of producing same: U.S. patent: 2679172 A, priority date: 16.03.1951(2679172)
4. Nakagawa T, Suzuki K (1981) A low cost blanking tool with bainite steel sheet laminated. In: Alexander JM (ed) Proceedings of the twenty-first international machine tool design and research conference. Macmillan Education UK, London, pp 129–138
5. Nakagawa T, Kunieda M, Liu S-D (1985) Laser cut sheet laminated forming dies by diffusion bonding. In: Tobias SA (ed) Proceedings of the twenty-fifth international machine tool design and research conference. Macmillan Education UK, London, pp 505–510
6. Weaver WR (1991) Process for the manufacture of laminated tooling: U.S. patent: 5031483 A, priority date: 06.10.1989
7. Yoo S, Walczyk DF (2005) Advanced design and development of profiled edge laminae tools. J Manuf Process 7:162–173
8. Walczyk DF, Hardt DE (1998) Rapid tooling for sheet metal forming using profiled edge laminations-design principles and demonstration. J Manuf Sci Eng 120:746. https://doi.org/10.1115/1.2830215
9. Kleiner M, Krux R (2001) Entwicklung eines Verfahrens zur schnellen Herstellung von Tief- und Streckziehwerkzeugen aus Blechlamellen für die Prototypen- und Kleinserienfertigung (Rapid Tooling). Forschung für die Praxis // Stahl-Zentrum Düsseldorf P, vol 384. Verl. und Vertriebsges. mbH, Düsseldorf
10. Techel A (2005) Melato - metal laminated tooling: Werkzeugfertigung durch Blechpaketierung; Ergebnisbericht zum Verbundvorhaben: Qualifikation innovativer Fertigungstechnologien zur flexiblen Fertigung von großformatigen und komplex geformten Werkzeugen mit seriennahen Eigenschaften ; BMBF-Rahmenkonzept Forschung für die Produktion von morgen. Fraunhofer IRB Verl., Stuttgart
11. Yoon SH, Na SJ (2005) Application of laser joining process for elimination of stair steps in steel laminate tooling. Int J Adv Manuf Technol 25:154–159. https://doi.org/10.1007/s00170-003-1815-7
12. Hiegemann L, Agarwal C, Weddeling C et al. (2016) Reducing the stair step effect of layer manufactured surfaces by ball burnishing. In: 19th ESAFORM. Springer Berlin Heidelberg, 190002–1–190002–6
13. DIN 52900: DIN EN ISO/ASTM 52900 (2021) Fundamentals and vocabulary. Beuth Verlag GmbH, Berlin
14. Erasenthiran P, O'Neill W, Steen WM (1997) Investigation of normal and slant laser cutting using cw and pulsed CO2 laser for laminated object manufacturing techniques. In: Beckmann LHJF (ed) Lasers in Material Processing. SPIE, pp 48–57
15. Hölker-Jäger R, Tekkaya AE (2018) Verfahren zur Reduzierung des Treppenstufeneffekts bei aus Blechen geschichteten Bauteilen oder Werkzeugen mittels additiver Auftragsverfahren und umformtechnischer Nachbearbeitung: German patent: DE102018004294 A, priority date: 22.09.2014
16. Dardaei Joghan H, Hahn M, Sehrt JT et al (2022) Hybrid additive manufacturing of metal laminated forming tools. CIRP Ann. https://doi.org/10.1016/j.cirp.2022.03.018
17. Souza AM, Ferreira R, Barragán G et al (2021) Effects of laser polishing on surface characteristics and wettability of directed energy-deposited 316L stainless steel. J Materi Eng Perform 30:6752–6765. https://doi.org/10.1007/s11665-021-05991-y
18. De Los B, Rios GA, Ferreira R, Mariani FE et al (2022) Study of the surface roughness of a remanufactured bimetallic AISI 1045 and 316L SS part obtained by hybrid manufacturing (DED/HSM). Int J Adv Manuf Technol. https://doi.org/10.1007/s00170-022-09179-z
19. Tebaay LM, Hahn M, Tekkaya AE (2020) Distortion and dilution behavior for laser metal deposition onto thin sheet metals. Int J of Precis Eng Manuf-Green Tech 7:625–634. https://doi.org/10.1007/s40684-020-00203-9
20. Rangaswamy P, Griffith ML, Prime MB et al (2005) Residual stresses in LENS® components using neutron diffraction and contour method. Mater Sci Eng A 399:72–83. https://doi.org/10.1016/j.msea.2005.02.019
21. Wang Z, Denlinger E, Michaleris P et al (2017) Residual stress mapping in Inconel 625 fabricated through additive manufacturing: method for neutron diffraction measurements to validate thermomechanical model predictions. Mater Des 113:169–177. https://doi.org/10.1016/j.matdes.2016.10.003
22. Li C, Liu ZY, Fang XY et al (2018) Residual stress in metal additive manufacturing. Procedia CIRP 71:348–353. https://doi.org/10.1016/j.procir.2018.05.039
23. Jiang J, Lian G, Xu M et al (2016) Influence of preheating temperature on mechanical properties of laser cladding layer. In: Volume 1: Proceedings of the ASME 2016 international manufacturing science and engineering conference. Am Soc Mech Eng. https://doi.org/10.1115/MSEC2016-8718
24. Alimardani M, Fallah V, Khajepour A et al (2010) The effect of localized dynamic surface preheating in laser cladding of Stellite

1. Surf Coat Technol 204:3911–3919. https://doi.org/10.1016/j.surfcoat.2010.05.009
25. Ding C, Cui X, Jiao J et al. (2018) Effects of substrate preheating temperatures on the microstructure, properties, and residual stress of 12CrNi2 prepared by laser cladding deposition technique. Materials (Basel) 11.https://doi.org/10.3390/ma11122401
26. Meng W, Zhang W, Zhang W et al (2020) Fabrication of steel-Inconel functionally graded materials by laser melting deposition integrating with laser synchronous preheating. Opt Laser Technol 131:106451. https://doi.org/10.1016/j.optlastec.2020.106451
27. DIN EN ISO 4287 DIN EN ISO 4287 (2010). Geometrische Produktspezifikation (GPS) - Oberflächenbeschaffenheit: Tastschnittverfahren - Benennungen, Definitionen und Kenngrößen der Oberflächenbeschaffenheit
28. DIN EN ISO 25178 DIN EN ISO 25178–2 (2012). Geometrische Produktspezifikation (GPS)-Oberflächenbeschaffenheit: Flächenhaft - Teil 2: Begriffe und Oberflächen-Kenngrößen
29. Townsend A, Senin N, Blunt L et al (2016) Surface texture metrology for metal additive manufacturing: a review. Precis Eng 46:34–47. https://doi.org/10.1016/j.precisioneng.2016.06.001
30. Jiang X, Scott P, Whitehouse D et al (2007) Paradigm shifts in surface metrology. Part II. The current shift. Proc R Soc A 463:2071–2099. https://doi.org/10.1098/rspa.2007.1873
31. Ren K, Chew Y, Fuh J et al (2019) Thermo-mechanical analyses for optimized path planning in laser aided additive manufacturing processes. Mater Des 162:80–93. https://doi.org/10.1016/j.matdes.2018.11.014
32. DIN EN ISO 6892 DIN EN ISO 6892 (2009) Metallische Werkstoffe - Zugversuch - Teil1: Prüfverfahren bei Raumtemperatur, Beuth Verlag GmbH, Berlin
33. DIN 50125 DIN 50125 (2009). Prüfung metallischer Werkstoffe-Zugproben, Beuth Verlag GmbH, Berlin
34 Milella PP (2013) Fatigue and corrosion in metals. Springer Milan, Milano
35. Kumaran M, Senthilkumar V (2021) Experimental characterization of stainless steel 316L alloy fabricated with combined powder bed fusion and directed energy deposition. Weld World 65:1373–1388. https://doi.org/10.1007/s40194-021-01117-z
36. Ya W, Pathiraj B, Liu S (2016) 2D modelling of clad geometry and resulting thermal cycles during laser cladding. J Mater Process Technol 230:217–232. https://doi.org/10.1016/j.jmatprotec.2015.11.012
37. Hao X, Dong H, Li S et al (2018) Lap joining of TC4 titanium alloy to 304 stainless steel with fillet weld by GTAW using copper-based filler wire. J Mater Process Technol 257:88–100. https://doi.org/10.1016/j.jmatprotec.2018.02.020